Chemical Engineering Journal 456 (2023) 140930

Contents lists available at ScienceDirect

Chemical Engineering Journal

journal homepage: www.elsevier.com/locate/cej

Fluoroalkane modified cationic polymers for personalized mRNA cancer vaccines

Junyan Li [a,b], Yuanyuan Wu [a,b], Jian Xiang [d], Hairong Wang [c], Qi Zhuang [a,b], Ting Wei [e], Zhiqin Cao [a,b], Qingyang Gu [d,*], Zhuang Liu [a,b,*], Rui Peng [a,b,*]

[a] Institute of Functional Nano & Soft Materials (FUNSOM), Soochow University, 199 Ren'ai Rd, Suzhou, Jiangsu 215123, China
[b] Jiangsu Key Laboratory for Carbon-Based Functional Materials and Devices, Soochow University, 199 Ren'ai Rd, Suzhou, Jiangsu 215123, China
[c] Children's Hospital of Soochow University, Suzhou, Jiangsu 215006, China
[d] WuXi AppTec (Suzhou) Co., Ltd., 1336 Wuzhong Avenue, Wuzhong District, Suzhou 215104, China
[e] InnoBM Pharmaceuticals Co., Ltd., Suzhou, Jiangsu 215000, China

ARTICLE INFO

Keywords:
Fluoropolymer
mRNA Delivery
Antigen presentation
Personalized mRNA cancer vaccine
Cancer immunotherapy

ABSTRACT

Messenger RNA (mRNA) vaccines, while demonstrating great successes in the fight against COVID-19, have been extensively studied in other areas such as personalized cancer immunotherapy based on tumor neoantigens. In addition to the design of mRNA sequences and modifications, the delivery carriers are also critical in the development of mRNA vaccines. In this work, we synthesized fluoroalkane-grafted polyethylenimine (F-PEI) for mRNA delivery. Such F-PEI could promote intracellular delivery of mRNA and activate the Toll-like receptor 4 (TLR4)-mediated signaling pathway. The nanovaccine formed by self-assembly of F-PEI and the tumor antigen-encoding mRNA, without additional adjuvants, could induce the maturation of dendritic cells (DCs) and trigger efficient antigen presentation, thereby eliciting anti-tumor immune responses. Using the mRNA encoding the model antigen ovalbumin ($mRNA^{OVA}$), our F-PEI-based $mRNA^{OVA}$ cancer vaccine could delay the growth of established B16-OVA melanoma. When combined with immune checkpoint blockade therapy, the F-PEI-based MC38 neoantigen mRNA cancer vaccine was able to suppress established MC38 colon cancer and prevent tumor reoccurrence. Our work presents a new tool for mRNA delivery, promising not only for personalized cancer vaccines but also for other mRNA-based immunotherapies.

1. Introduction

Cancer vaccines, which trigger tumor-specific cell-mediated immunity to recognize and kill cancer cells, are one of the most interesting approaches in cancer immunotherapy [1–3]. mRNA-based vaccines are a promising vaccine platform for several reasons [4,5]. Firstly, mRNA is delivered into the cytosol for rapid production of large quantity of endogenous protein or peptide antigens, which are processed by the proteasome and presented to the cell surface by the major histocompatibility complex class I (MHC I) to activate $CD8^+$ T cells that are thought to play a key role in the antitumor immunity [6–8], whereas exogenous peptide/protein antigens are mainly been processed in the lysosome and presented via MHC II, inducing humoral immunity [9]. Therefore, compared with peptide/protein vaccines, mRNA vaccines may induce stronger cellular immune responses for antitumor immunity. Secondly, compared with protein antigens, mRNA antigens have stronger immunogenicity and possess intrinsic adjuvant properties, which could further enhance immune responses [10]. Thirdly, compared with DNA vaccines, mRNA vaccines only need to be internalized into the cytoplasm for translation, without raising the risk of gene integration or other safety issues [11].

However, due to the abundance of RNases and the difficulty of mRNA molecules in entering cells, biocompatible delivery carriers that can improve the mRNA stability and transport mRNA into antigen-presenting cells (APCs) are essential in the development of mRNA vaccines [12–14]. Currently, lipid nanoparticles (LNPs) have demonstrated great successes as the delivery system in the fabrication of mRNA vaccines [15–17]. However, LNPs usually are composed by a variety of different lipid components with rather complicated compositions. Moreover, state-of-art microfluidic devices are usually required in the fabrication processes to produce LNP-based mRNA vaccines [18]. Developing new mRNA delivery carriers with simple composition and

* Corresponding authors at: Institute of Functional Nano & Soft Materials (FUNSOM), Soochow University, 199 Ren'ai Rd, Suzhou, Jiangsu 215123, China.
E-mail addresses: gu_qingyang@wuxiapptec.com (Q. Gu), zliu@suda.edu.cn (Z. Liu), rpeng@suda.edu.cn (R. Peng).

https://doi.org/10.1016/j.cej.2022.140930
Received 1 September 2022; Received in revised form 12 November 2022; Accepted 10 December 2022
Available online 12 December 2022

easy preparation process would still be of great interests for mRNA-based biotechnology.

An effective mRNA delivery carrier should be able to pack and protect the mRNA from enzymatic degradation, to transport the mRNA either directly into the cytosol or via escaping from the lysosome, and finally to release the mRNA cargo to the cellular translation machinery. Therefore, both the affinity of the carrier towards the mRNA cargo and the interaction(s) of the carrier with the target cell would contribute to its delivery efficiency. Fluorine-containing amphiphiles have been reported to show promising gene and protein delivery effects [19–22]. Fluorinated compounds with both hydrophobic and lipophobic features show a high tendency of phase separation in both polar and non-polar environments [23,24], enabling their penetration across the lipid bilayer of cell membranes as well as endosomal/lysosomal membranes [25,26]. In our previous work, we reported that a fluoroalkane modified polyethylenimine (PEI) with a molecular weight of 25 kDa (F-PEI$_{25\ kDa}$), while serving as an agonist for the Toll-like receptor 4 (TLR4)-mediated signaling pathway, could self-assemble with protein or peptide antigens to form nanovaccines without the need of additional adjuvants [27]. However, regular PEI with high molecular weight possesses certain cytotoxicity, thus limiting its potential in bio-applications [28,29].

Here, a low molecular weight (1.8 kDa) PEI with low cytotoxicity was chosen for further optimization in this study. Two fluoroalkane-grafted PEI polymers (F-PEI$_{1.8\ kDa}$) were synthesized for efficient mRNA delivery and TLR4 activation. By simply mixing F-PEI with the mRNA encoding tumor antigens (Ag), without additional adjuvants, we obtained F-PEI/mRNA^{Ag} nanovaccines which could promote high level of dendritic cells (DCs) activation and MHC I antigen processing and presentation by APCs, subsequently inducing antigen-specific CD8$^+$ T cell immune responses to effectively inhibit the growth of established B16-OVA melanoma tumors. We further demonstrated that using the mRNA encoding neoantigens of MC38 tumors, F-PEI-based personalized nanovaccine, in combination with the immune checkpoint inhibitors, could eradicate established tumors (Fig. 1). This work presents a new type of mRNA delivery vector that may be of great interests to the development of mRNA-based personalized cancer vaccines as well as other mRNA-based immunotherapies.

2. Experimental

2.1. Materials

Branched polyethylenimine (MW 1.8 kDa) was purchased from Sigma-Aldrich (St. Louis, MO). 3-(perfluorohex-1-yl)-1,2-propenoxide was purchased from J&K Scientific (Shanghai, China). Firefly-luciferase and OVA expression mRNAs were obtained from Trilink. MC38 neoantigen expression mRNA was commissioned to construct by Stemirna (Shanghai, China). The firefly-luciferase mRNA labeled with the

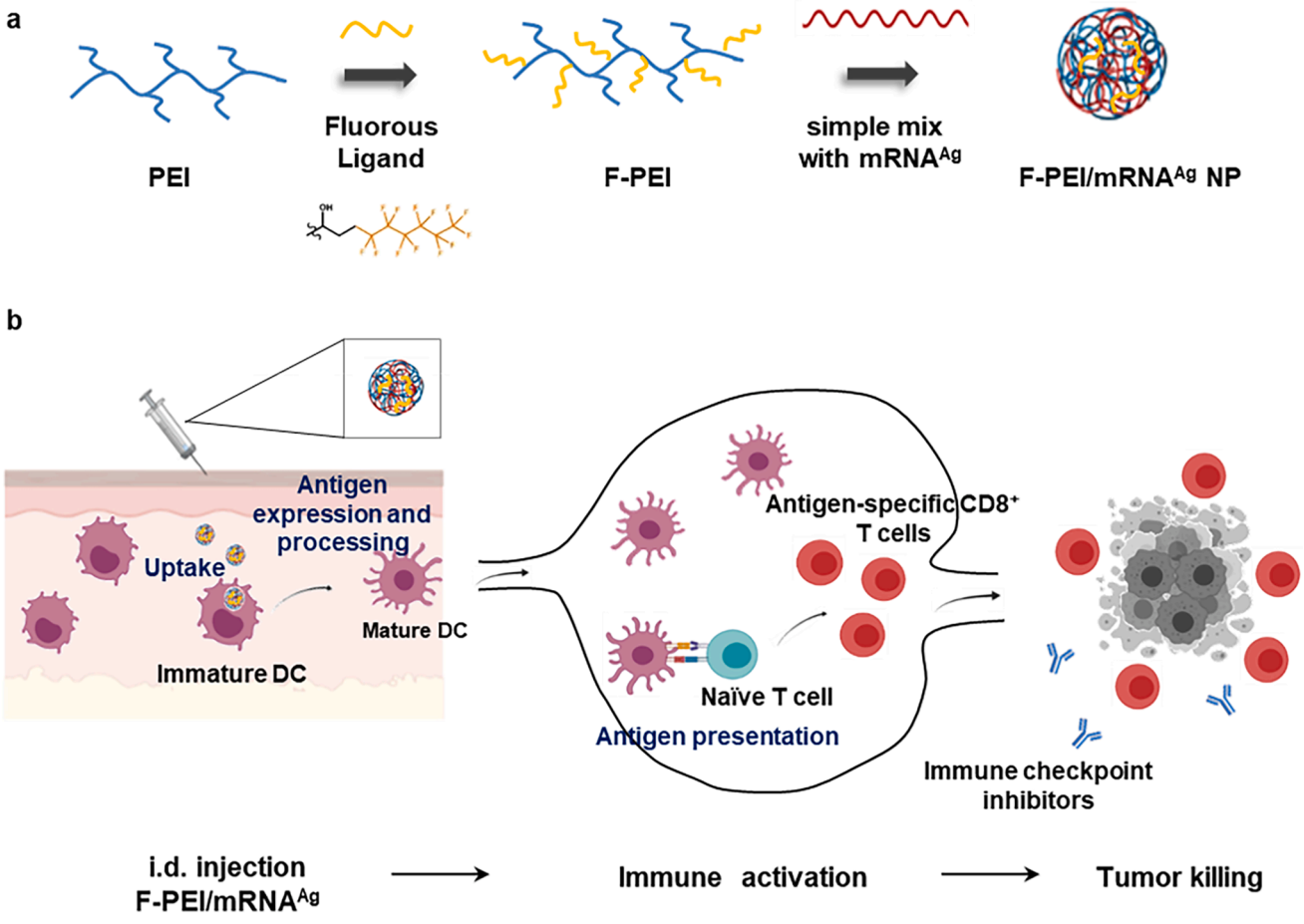

Fig. 1. Design of the F-PEI/mRNA nanovaccine platform for cancer treatment. (a) Schematic illustration showing the preparation of F-PEI/mRNA nanovaccine. F-PEI was synthesized by grafting fluorine ligands on PEI (MW 1.8 kDa), and then mixed with the mRNA encoding antigen (Ag) to form F-PEI-based mRNA nanovaccine (F-PEI/mRNA^{Ag}). (b) After administration, F-PEI/mRNA^{Ag} nanovaccine is taken up by dendritic cells (DCs), to promote antigen presentation and maturation of DCs. Then activated DCs would migrate to the draining lymph nodes, triggering robust antigen-specific CD8$^+$ T cell responses. Activated CD8$^+$ T cells would then recognize and kill target cancer cells and exert powerful antitumor efficacy. Combining with immune checkpoint inhibitors would further enhance the efficacy of F-PEI-based mRNA nanovaccine to eliminate established tumors. Ag, antigen. i.d., intradermal.

fluorophore Cy5 was obtained from APExBIO. Lipofectamine MessengerMAX was purchased from Invitrogen.

2.2. Animals and cells

Female C57BL/6 mice (6–8 weeks) were purchased from Nanjing Pengsheng Biological Technology Co., ltd. Female OT-I transgenic mice (6–8 weeks) were a kind gift from Prof. Xuefeng Wang, Soochow University. All animal experiments were performed according to the guidelines for the protection of animal life and protocols approved by Laboratory Animal Ethics Committee in Soochow University. B16-OVA cells (a gift from Prof. Yuhui Huang, Soochow University), RAW264.7 cells (obtained from American Type Culture Collection) were cultured in Dulbecco's modifed Eagle medium (DMEM) with 10 % fetal bovine serum (FBS) and 1 % penicillin sulfate and streptomycin (PS) at 37 °C in 5 % CO_2. DC2.4 cells (a gift from Prof. Chao Wang, Soochow University), MC38 cells (obtained from American Type Culture Collection) were cultured in Roswell Park Memorial Institute (RPMI) 1640 medium 10 % FBS and 1 % PS at 37 °C in 5 % CO_2. HEK-Dual mTLR4 (NF/IL8) cells (obtained from InvivoGen) were cultured in DMEM with 10 % FBS and 1 % PS supplemented with 100 μg mL^{-1} Hygromycin B Gold (InvivoGen) and 50 μg mL^{-1} Zeocin (InvivoGen) at 37 °C in 5 % CO_2.

2.3. Synthesis of F-PEI

Epoxides of fluoroalkanes were added dropwisely into $PEI_{1.8k}$ in methanol at different molar ratios (75:1 or 100:1). The mixture was stirred at room temperature for 48 h, then the products were purified by intensive dialysis against methanol and double distilled water (molecular weight cut off 1000 Da). The products were collected and lyophilized under vacuum to obtain F-PEI.

2.4. In vitro cytotoxicity assessment

DC2.4 cells or RAW264.7 macrophages were seeded into 96-well plates at 5×10^4 cells per well and incubated with different concentrations of F-PEI or PEI for 24 h, and relative cell viability was measured by standard MTT assay.

2.5. Nucleic acid condensation ability assay

Agarose Gel Electrophoresis (AGE) was used to verify the ability of F-PEI to condense mRNA. F-PEI/mRNA complexes at various w/w ratios (from 0.25 to 2) were prepared, added with 2 × RNA loading dye (Solarbio), heat-treated at 65 °C for 8 min, loaded onto a 1 % agarose denaturing gel containing GelRed dye (Beyotime), and then electrophoresed at 125 V for 30 min. The electrophoretic band was imaged by using Amersham Imager 600 UV System.

2.6. Characterization of F-PEI/mRNA

The synthesized F-PEI was mixed with mRNA in deionized water at a mass ratio of 1:1 for 15 min. The size and zeta potential of the formed F-PEI/mRNA NPs were measured using a Zetasizer Nano ZS (Malvern Instruments). The morphology of the NPs was observed with a FEI TF20 transmission electron microscope.

2.7. In vivo mRNA expression assay

The F-PEI/$mRNA^{Luc}$ (10 μg $mRNA^{Luc}$ per mouse) was intradermally injected at the tail base of each C57BL/6 mouse, followed by intraperitoneal injection of 0.2 mL of d-luciferin (1.5 μg mL^{-1}) after 6 h and 24 h. After 15 min of reaction, the mice were subjected to bioluminescence assays using IVIS Kinetic Imaging System (Perkin Elmer).

2.8. BMDC activation and antigen presentation

For *in vitro* DC maturation experiments, BMDCs were plated at 10^6 cells per well in a 24-well plate and incubated with $mRNA^{OVA}$, F-PEI/$mRNA^{OVA}$ or Lipofectamine MessengerMAX/$mRNA^{OVA}$ ($mRNA^{OVA}$ = 3 μg mL^{-1}, the w/w ratio of material and $mRNA^{OVA}$ was 1:1). After 24 h incubation, BMDCs were harvested and washed with FACS buffer (1 % FBS in PBS), and incubated with anti-CD16/32 at 4 °C, then stained with anti-CD11c-FITC, anti-CD80-APC and anti-CD86-PE for DC maturation analysis, or anti-CD11c-APC and anti-SIINFEKL/H-$2K^b$-PE for antigen presentation analysis.

2.9. In vitro mRNA cellular uptake

To assess the cellular uptake of mRNA by BMDCs, 10^6 BMDCs were plated in 24-well plate and incubated with Cy5-labelled $mRNA^{Luc}$ (Cy5-$mRNA^{Luc}$), F_{13}-$PEI_{1.8k}$-1/Cy5-$mRNA^{Luc}$, F_{13}-$PEI_{1.8k}$-2/Cy5-$mRNA^{Luc}$ for 6 h (Cy5-$mRNA^{Luc}$ = 1 μg mL^{-1}, The w/w ratio of material and $mRNA^{Luc}$ was 1:1). BMDCs were harvested and added with trypan blue to quench the extracellular fluorescence. After washing for three times, BMDCs were incubated with anti-CD16/32 for 15 min at 4 °C before being stained with anti-CD11c-FITC, and then analyzed using flow cytometer (BD Accurit C6 Plus).

2.10. In vitro $CD8^+$ T-cell priming assay

BMDCs were incubated with F-PEI/$mRNA^{OVA}$ NPs. Then the treated BMDCs were washed by PBS containing 0.1 % BSA. $CD8^+$ T lymphocytes were negatively selected from the spleen of OT-I mice by magnetic separation (MACS system, Miltenyi Biotec) according to the manufacturer's instructions and stained with the CellTrace CFSE Cell Proliferation Kit (Invitrogen) according to the experimental protocol. The treated BMDCs (10^5 mL^{-1}) were then mixed with CFSE-stained splenic $CD8^+$ T cells at a ratio of 1:10, and incubated in round-bottom 96-well plates (Beyotime) for 72 h. Cells were washed by FACS buffer, before being incubated with anti-CD16/32 at 4 °C then stained with anti-CD3-PerCP for flow cytometer measurement.

2.11. Detection of cytokine

The supernatant after incubation in $CD8^+$ T-cell priming assay was collected, and the secretion level of IFN-γ in the cell supernatant was detected by enzyme-linked immunosorbent assay (ELISA). The experimental steps were performed according to the instructions of the ELISA kit (Invitrogen).

2.12. Lymph node analysis

C57BL/6 mice were immunized with PBS, $mRNA^{OVA}$ or F-PEI/$mRNA^{OVA}$ by intradermal injection on Day 0. The injected dose of $mRNA^{OVA}$ per mouse was 10 μg. On Day 3 after mouse immunization, we assessed DC maturation and antigen presentation in mouse inguinal lymph nodes (LNs). LNs from immunized mice were treated by mechanical disruption, then filtered through 300-mesh nylon mesh to obtain single-cell suspensions, which were incubated with anti-CD16/32 for 15 min at 4 °C before being stained with anti-CD11c-FITC, anti-CD86-PE and anti-CD80-APC for DC maturation analysis, or anti-CD11c-APC and anti-SIINFEKL/H-2 K^b-PE for antigen presentation analysis.

2.13. Tetramer analysis and peptide re-stimulation of splenocytes

C57BL/6 mice were intradermally immunized with PBS, $mRNA^{OVA}$ or F-PEI/$mRNA^{OVA}$ on Day 0 and 7. On Day 14, the spleens of the immunized mice were minced and filtered with a 300 mesh cell strainer to obtain splenocytes, and then Red blood cells (RBCs) were lysed with RBC lysis buffer (Beyotime). Splenocytes were stained with PE-labelled

SIINFEKL-MHC I tetramer, anti-CD8-APC and anti-CD3-FITC, then analyzed the percentage of OVA-specific $CD8^+$ T cells using the tetramer staining assay following the standard protocol.

For enzyme linked immunospot assay (ELISPOT) analysis of IFN-γ spot-forming cells (BD Biosciences), 5×10^5 splenocytes were plated in each well and incubated with 10 μg mL^{-1} $OVA_{257–264}$ peptide (SIINFEKL), Reps1 peptide (AQLANDVVL), Dpagt1 peptide (SIIVFNLL) or Adpgk peptide (ASMTNMELM), respectively. The plates were kept at 37 °C in 5 % CO_2 for 24 h. Following the experimental protocol, an automated ELISPOT Plate Reader (AID iSpot) was used to determine the amount of IFN-γ spot-forming cells and the data were presented as spot-forming cells per half million cells.

To demonstrate the cellular responses, 10^6 immunized mice splenocytes were incubated with 10 μg mL^{-1} $OVA_{257-264}$ peptide (SIINFEKL) in the medium containing brefeldin A inhibitor and monensin inhibitor for 6 h. Cells were incubated with anti-CD16/32 antibody at 4 °C for 15 min, and then stained with anti-CD3e-FITC and anti-CD8a-APC at 4 °C for 30 min. Then the cells were stained anti-IFN-γ-PE according to the intracellular staining protocol before the flow cytometry measurement.

2.14. Hematoxylin and eosin (H&E) staining

C57BL/6 mice were intradermally treated two times with F_{13}-$PEI_{1.8k}$-1/$mRNA^{OVA}$ or F_{13}-$PEI_{1.8k}$-2/$mRNA^{OVA}$ at 1 week intervals. Mice were euthanized and collected major organs on Day 1, 7 and 21 after two vaccination. The major organs were fixed in 4 % paraformaldehyde solution, and then sectioned for H&E staining.

2.15. Treatment of the B16-OVA tumor model

C57BL/6 mice were subcutaneously inoculated with 5×10^5 B16-OVA cells on Day 0. Mice were intradermally treated with PBS, $mRNA^{OVA}$ or F-PEI/$mRNA^{OVA}$ on Day 4 and 11. The injected dose of $mRNA^{OVA}$ per mouse was 10 μg. The tumor growth were regularly measured and recorded: tumor volume = length × width × width/2. Mice were euthanized when the tumor volume reached 1500 mm^3.

2.16. Neoantigen mRNA vaccine combined with immune checkpoint inhibitor for tumor therapy

C57BL/6 mice were subcutaneously injected with 10^6 MC38 colon cancer cells on Day 0. Tumor-bearing mice were randomly divided into 4 groups and treated with different treatments: (1) PBS, (2) anti-PD-1, (3) F_{13}-$PEI_{1.8k}$-1/$mRNA^{MC38}$, (4) F_{13}-$PEI_{1.8k}$-1/$mRNA^{MC38}$ + anti-PD-1. Mice were intradermally immunized with F_{13}-$PEI_{1.8k}$-1/$mRNA^{MC38}$ on Days 8 and 15. The injected dose of $mRNA^{MC38}$ per mouse was 10 μg. On Day 9 and 16, mice were intravenously injected with anti-PD-1 (20 μg per mouse). On Day 12 and 19, mice were intravenously injected with anti-PD-1 (10 μg per mouse). Mice were euthanized when the tumor volume reached 1000 mm^3.

For tumor rechallenge experiment, tumor-eliminated mice treated with neoantigen mRNA nanovaccine combined with immune checkpoint inhibitors were subcutaneously injected with 5×10^5 MC38 cells on Day 60. The tumor growth was monitored and recorded to evaluate the immune memory effect.

2.17. $CD8^+$ T cell depletion

Each C57BL/6 mouse was subcutaneously injected with 10^6 MC38 cells on Day 0. The tumor-bearing mice were randomly divided into 4 groups and treated with different methods: (1) mouse-IgG (as Control, Southern Biotech), (2) anti-mouse-CD8a (BioXcell), (3) F_{13}-$PEI_{1.8k}$-1/$mRNA^{MC38}$ + anti-PD-1 + anti-mouse-CD8a, (4) F_{13}-$PEI_{1.8k}$-1/$mRNA^{MC38}$ + anti-PD-1 + mouse-IgG. On Day 7, 10 and 13, mice were intravenously injected with anti-mouse-CD8a or mouse-IgG antibody (20 μg per mouse). On Day 8, mice were intradermally immunized with F_{13}-$PEI_{1.8k}$-1/$mRNA^{MC38}$. On Day 9, mice were intravenously injected with anti-PD-1 (20 μg per mouse). On Day 12, mice were intravenously injected with anti-PD-1 (10 μg per mouse). The peripheral blood of mice was collected on Day 10, and the depletion of $CD8^+$ T cells was detected by flow cytometry.

3. Results and discussion

3.1. Characterization and the mRNA delivery efficiency of fluoropolymers

Branched PEI (MW 1.8 kDa) was grafted with fluoroalkanes (3-(perfluoro-*n*-hexyl)-1,2-propenoxide, F_{13}) via amine-epoxide reaction [22]. The F_{13} ligand was mixed with PEI at 2 different feed ratios: 75:1, 100:1, and the obtained materials were named as F_{13}-$PEI_{1.8k}$-1 and F_{13}-$PEI_{1.8k}$-2 with the fluorine contents of 35.98 % and 40.36 %, respectively.

Firstly, we verified the ability of F-PEI to condense nucleic acids by agarose gel electrophoresis. The two F-PEIs were simply mixed with mRNA at increasing w/w ratios. Both F_{13}-$PEI_{1.8k}$-1 and F_{13}-$PEI_{1.8k}$-2 could successfully encapsulate mRNA at a very low ratio to prevent its leakage by forming particles (Fig. 2a), demonstrated by the disappearance of the free mRNA band. The cytotoxicity of F-PEIs was also explored. Cell viability was analyzed after incubating RAW264.7 macrophages and DC2.4 cells with the two F-PEIs or bare $PEI_{1.8k}$. Both F-PEIs showed comparable low cytotoxicity with bare $PEI_{1.8k}$ (Supplementary Fig. S1), demonstrating that the fluorine modification did not affect the biocompatibility. Considering no obvious toxicity could be observed at 10 μg mL^{-1} (Supplementary Fig. S1), the w/w ratio of F_{13}-$PEI_{1.8k}$-1/mRNA and F_{13}-$PEI_{1.8k}$-2/mRNA was set at 1:1 accordingly giving a working concentration of 3–10 μg mL^{-1}. At this ratio, the particle sizes were both about 280 nm in hydrodynamic diameter (Fig. 2b) with spherical shape under TEM (Fig. 2c), and their zeta potentials were approximately −6.5 mV and −12.3 mV, respectively (Fig. 2d).

We next investigated the mRNA cellular delivery efficiency of F-PEIs *in vitro*. mRNA encoding firefly luciferase ($mRNA^{Luc}$) was labeled with Cyanine 5 (Cy5) fluorescent dye (Cy5-$mRNA^{Luc}$) for intracellular tracking. Compared with free Cy5-$mRNA^{Luc}$, both F_{13}-$PEI_{1.8k}$-1/Cy5-$mRNA^{Luc}$ and F_{13}-$PEI_{1.8k}$-2/Cy5-$mRNA^{Luc}$ promoted mRNA uptake by mouse bone marrow-derived dendritic cells (BMDCs) (Fig. 2e & 2f), indicating that F_{13}-$PEI_{1.8k}$-1 and F_{13}-$PEI_{1.8k}$-2 could significantly improve the mRNA entry efficiency, and the mRNA delivery efficiency of F_{13}-$PEI_{1.8k}$-1 was significantly higher than that of F_{13}-$PEI_{1.8k}$-2.

The mRNA delivery efficacy of F-PEI was also explored *in vivo*. F-PEI/$mRNA^{Luc}$ was intradermally injected at the tail base of mice, and the bioluminescence intensities at the injection site were evaluated after intraperitoneal injection of d-luciferin. The expression of luciferase was recorded at 6 h and 24 h post injection. Based on the bioluminescence intensities, it was found that F_{13}-$PEI_{1.8k}$-1 showed better *in vivo* mRNA delivery efficiency than F_{13}-$PEI_{1.8k}$-2 (Fig. 2g & 2 h), consistent with their abilities of mRNA packing and cellular delivery.

3.2. DC activation and OVA-specific T cell immune responses

The maturation of DCs was essential for antigen presentation and subsequent initiation of T cell immune responses (Fig. 3a). BMDCs were pulsed with $mRNA^{OVA}$, F_{13}-$PEI_{1.8k}$-1/$mRNA^{OVA}$, F_{13}-$PEI_{1.8k}$-2/$mRNA^{OVA}$ or Lipofectamine MessengerMAX/$mRNA^{OVA}$, the latter of which was a commercial mRNA transfection reagent. It was found that F_{13}-$PEI_{1.8k}$-1/$mRNA^{OVA}$ and F_{13}-$PEI_{1.8k}$-2/$mRNA^{OVA}$ treated BMDCs showed a high up-regulation in co-stimulatory molecules (CD80 and CD86) compared to the control group and the $mRNA^{OVA}$ group, indicating significantly stimulated maturation of BMDCs (Fig. 3b).

We then examined the antigen presentation efficiency via the MHC I pathway in BMDCs treated with F-PEI/$mRNA^{OVA}$ NPs. Compared with the $mRNA^{OVA}$ group, F_{13}-$PEI_{1.8k}$-1/$mRNA^{OVA}$, F_{13}-$PEI_{1.8k}$-2/$mRNA^{OVA}$

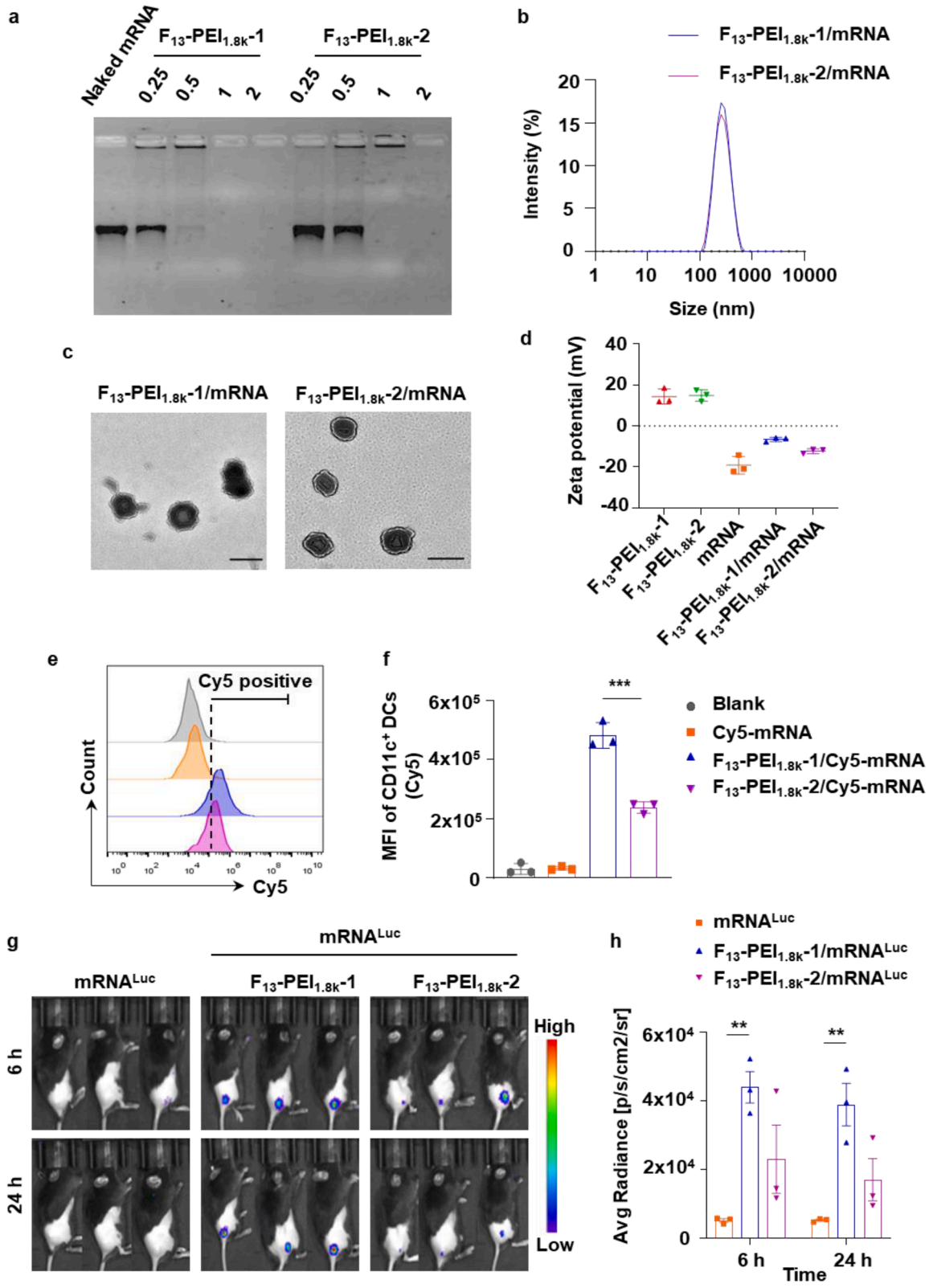

Fig. 2. Characterization and mRNA delivery efficiency of F-PEI. (a) Agarose gel electrophoresis of F-PEI/mRNA at different w/w ratios. (b) Dynamic light scattering analysis of F-PEI/mRNA. (c) Transmission electron microscopy imaging shown F_{13}-$PEI_{1.8k}$-1/mRNA and F_{13}-$PEI_{1.8k}$-2/mRNA. Scale bar = 200 nm. (d) Zeta potentials of the F_{13}-$PEI_{1.8k}$-1, F_{13}-$PEI_{1.8k}$-2, mRNA, F_{13}-$PEI_{1.8k}$-1/mRNA and F_{13}-$PEI_{1.8k}$-2/mRNA. (e&f) Representative flow cytometry plots (e) and the mean fluorescence intensity (MFI) of Cy5 (f) in BMDCs incubated with F-PEI/Cy5-$mRNA^{Luc}$ for 6 h. (g&h) F-PEI/$mRNA^{Luc}$ (10 μg $mRNA^{Luc}$ per mouse) was intradermally injected at the tail base of mice to evaluate the *in vivo* mRNA delivery efficiency, and the bioluminescence images (g) and statistical data (h) were recorded at 6 h and 24 h post injection. d,f, The data show mean ± standard deviation (n = 3). h, The data show mean ± standard error of mean (n = 3 mice per group). f,h, Statistical significance between the indicated groups was determined using two-sided unpaired t-tests. $^{**}P < 0.01$, $^{***}P < 0.001$.

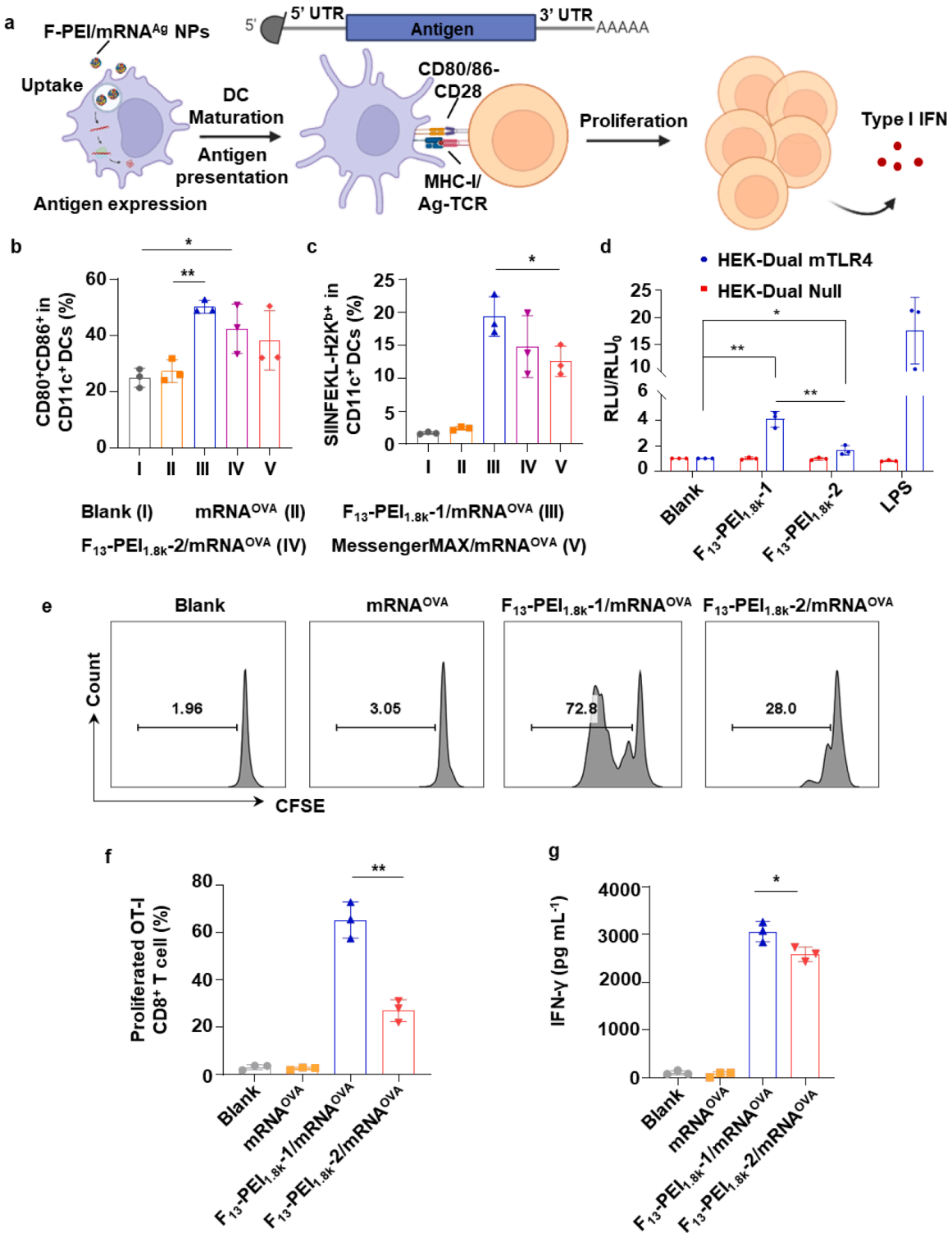

Fig. 3. Potent DC activation and antigen-specific T cell responses mediated by F-PEI/mRNA. (a) Schematic illustrating the mRNA encoding the specific antigen, the process of DC activation, antigen presentation and subsequent T cell proliferation. UTR, untranslated region. (b&c) Flow-cytometry analysis of $CD80^+CD86^+$ (b) and SIINFEKL-H-$2K^b$ (c) in BMDCs treated with $mRNA^{OVA}$, F-PEI/$mRNA^{OVA}$, or Lipofectamine MessengerMAX/$mRNA^{OVA}$. The $mRNA^{OVA}$ concentration was fixed at 3 μg mL^{-1}. (d) HEK-Dual Null (NF/IL8) cells (as control) and HEK-Dual mTLR4 (NF/IL-8) cells were stimulated with 10 μg mL^{-1} F_{13}-$PEI_{1.8k}$-1 or F_{13}-$PEI_{1.8k}$-2, respectively. Lipopolysaccharide (LPS, 2 μg mL^{-1}) was used as the positive control. After 12 h of incubation, activation of the TLR4 signaling pathway was determined by measuring the reporter Lucia luciferase activity. RLU, Relative light unit of treated groups. RLU0, RLU of the blank group. (e&f) Representative flow cytometry plots (e) and statistical data (f) showing proliferation of OT-I $CD8^+$ T cells after co-cultured with BMDCs pre-treated with $mRNA^{OVA}$ or F-PEI/$mRNA^{OVA}$. (g) Enzyme-linked immunosorbent assay (ELISA) measurement of IFN-γ in cell supernatants from the stimulated OT-I $CD8^+$ T cells in (f). The data show mean ± s.d. from 3 independent experiments (n = 3). b,c,d,f,g, Statistical significance between the indicated groups was determined using two-sided unpaired t-tests. $^*P < 0.05$, $^{**}P < 0.01$.

and Lipofectamine MessengerMAX/mRNA^{OVA} all could enhance the MHC I-associated SIINFEKL peptide presentation (Fig. 3c). More importantly, the F_{13}-$PEI_{1.8k}$-1/mRNA^{OVA} could induce a higher level of MHC I antigen presentation, and its efficiency was significantly higher than that of the Lipofectamine MessengerMAX/mRNA^{OVA} (Fig. 3c).

A recent study demonstrated that F-PEI with PEI molecular weight of 25 kDa could activate the TLR4 signaling pathway to stimulate DC activation[27]. TLR4 is an important member of the TLR protein family for pathogen recognition [30]. It has been reported that, by binding to its ligand, TLR4 promotes innate immune activation, and the activation of the TLR4 signaling pathway can enhance antigen-specific adaptive immune response, linking innate and adaptive immune responses [31]. Therefore, we next wanted to verify whether F-PEI with PEI molecular weight of 1.8 kDa could also possess the ability to activate the TLR4-mediated signaling pathway. As shown in Fig. 3d, the activation of TLR4 signaling pathway by F_{13}-$PEI_{1.8k}$-1 and F_{13}-$PEI_{1.8k}$-2 was confirmed using murine TLR4 (NF-κB-SEAP/KI-[IL-8]Lucia) dual-reporter HEK293 cells with stably transfected mouse TLR4 (mTLR4) MD-2/CD14 genes. Our results also showed that F_{13}-$PEI_{1.8k}$-1 could trigger TLR4 activation to a level significantly higher than F_{13}-$PEI_{1.8k}$-2 (Fig. 3d), suggested that F_{13}-$PEI_{1.8k}$-1, as an mRNA delivery vehicle, could be the better one for both cellular uptake enhancement and

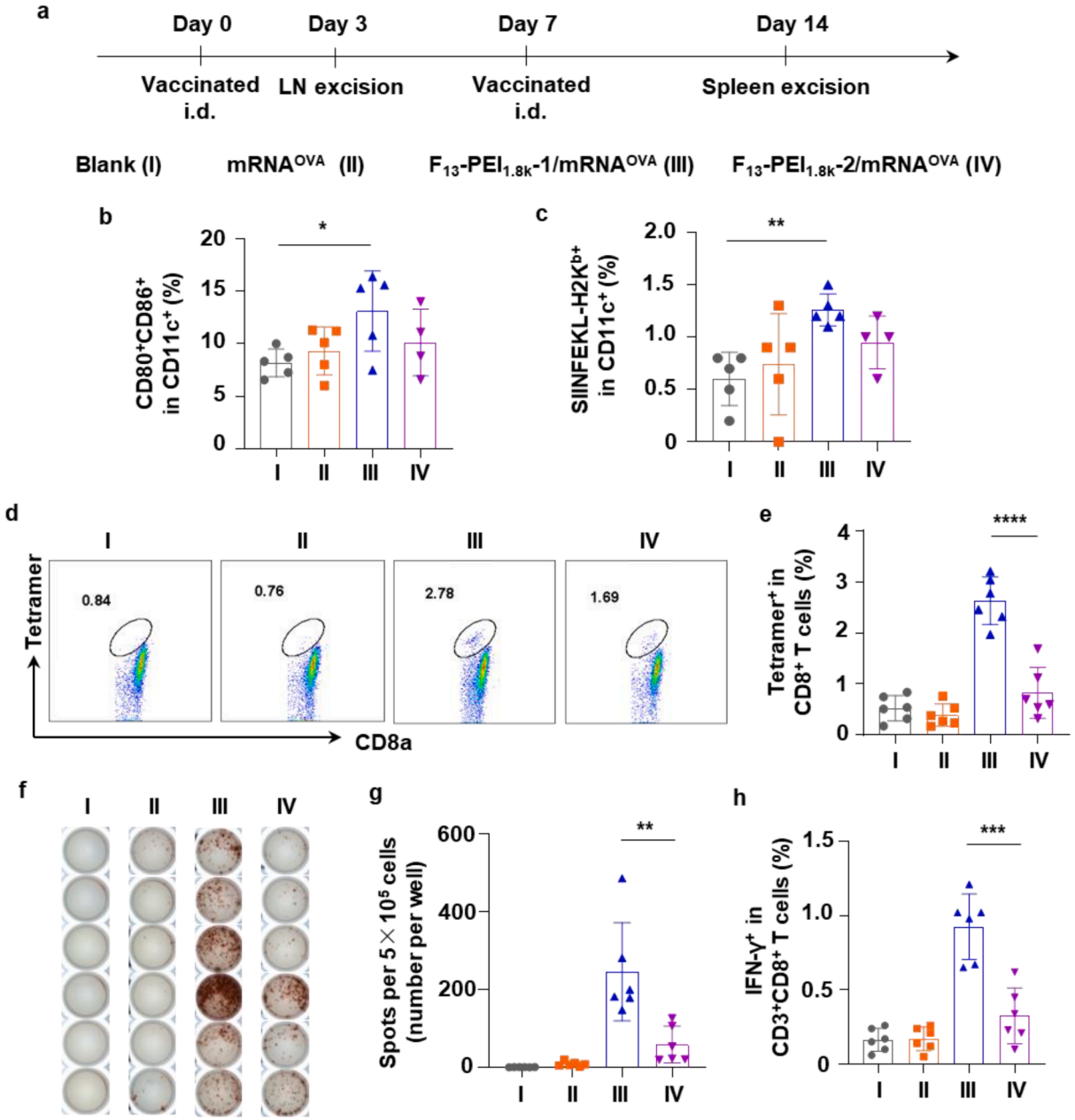

Fig. 4. In vivo immune stimulation by the F-PEI/mRNA^{OVA} nanovaccine. (a) Timeline of the experimental design to evaluate the *in vivo* immune responses triggered by the indicated formulations (mRNA^{OVA} or F-PEI/mRNA^{OVA}, 10 μg mRNA^{OVA} per mouse). (b&c) Proportions of CD80$^+$CD86$^+$ DCs (b) and SIINFEKL-H2K^{b+} (MHC I bound SIINFEKL$^+$) DCs (c) among DCs in LNs on Day 3 post one immunization. (d&e) Representative flow dot plots (d) and statistical data (e) of SIINFEKL-specific CD8$^+$ T cells in the spleen on Day 14 post two immunization by flow-cytometry analysis of MHC I/SIINFEKL tetramer$^+$CD8$^+$ T cells. (f&g) ELISPOT analysis of IFN-γ spot-forming cells (f) and statistical data (g) among splenocytes after *ex vivo* restimulation on Day 14 post two immunization. (h) The percentages of IFN-γ expression T cells in CD8$^+$ T cells from restimulated splenocytes on Day 14 post two immunization. b,c,e,g,h, The data show mean ± s.d. (b,c, n = 4–5 mice per group; e,g,h, n = 6 mice per group). Statistical significance between the indicated groups was determined using two-sided unpaired t-tests. *$P < 0.05$, **$P < 0.01$, ***$P < 0.001$, ****$P < 0.0001$. LNs, lymph nodes. i.d., intradermal.

immune stimulation.

The OT-I CD8$^+$ T cell contain transgenic T cell receptor designed to study the response of CD8$^+$ T cells to specific OVA antigen. Using *in vitro* OT-I CD8$^+$ T cell priming assay, BMDCs pre-treated with F_{13}-$PEI_{1.8k}$-1/$mRNA^{OVA}$ or F_{13}-$PEI_{1.8k}$-2/$mRNA^{OVA}$ could induce significant proliferation of OT-I CD8$^+$ T cells, while the BMDCs pre-treated with F_{13}-$PEI_{1.8k}$-1/$mRNA^{OVA}$ induced higher levels of OT-I CD8$^+$ T cell proliferation compared with those pre-treated with F_{13}-$PEI_{1.8k}$-2/$mRNA^{OVA}$ (Fig. 3e & 3f). Furthermore, for those CD8$^+$ T cells activated by BMDCs pre-treated with F-PEI/$mRNA^{OVA}$, a significant increase in the secretion of interferon-γ (IFN-γ) was also observed (Fig. 3g). Again, the above data indicated that F_{13}-$PEI_{1.8k}$-1/$mRNA^{OVA}$ NPs exhibited a better ability to activate BMDCs and trigger subsequent OVA-specific T cell responses.

3.3. *In vivo* stimulation of robust immune responses

Next, the immunization efficacy of the F-PEI/$mRNA^{OVA}$ vaccine was evaluated *in vivo*. C57BL/6 mice were intradermally injected with different formulations, the activation and antigen presentation of DCs in the inguinal lymph nodes of the mice were detected on Day 3 (Fig. 4a). Compared with the control group, in the lymph nodes of mice immunized with F_{13}-$PEI_{1.8k}$-1/$mRNA^{OVA}$, the proportion of DCs with up-regulated expression of the co-stimulatory molecules CD80/CD86 was significantly increased, and the MHC I antigen presentation of the model antigen OVA was also significantly increased (Fig. 4b & 4c).

After C57BL/6 mice were immunized twice with indicated formulations at 1 week intervals, the frequency of OVA-specific CD8$^+$ T cells in

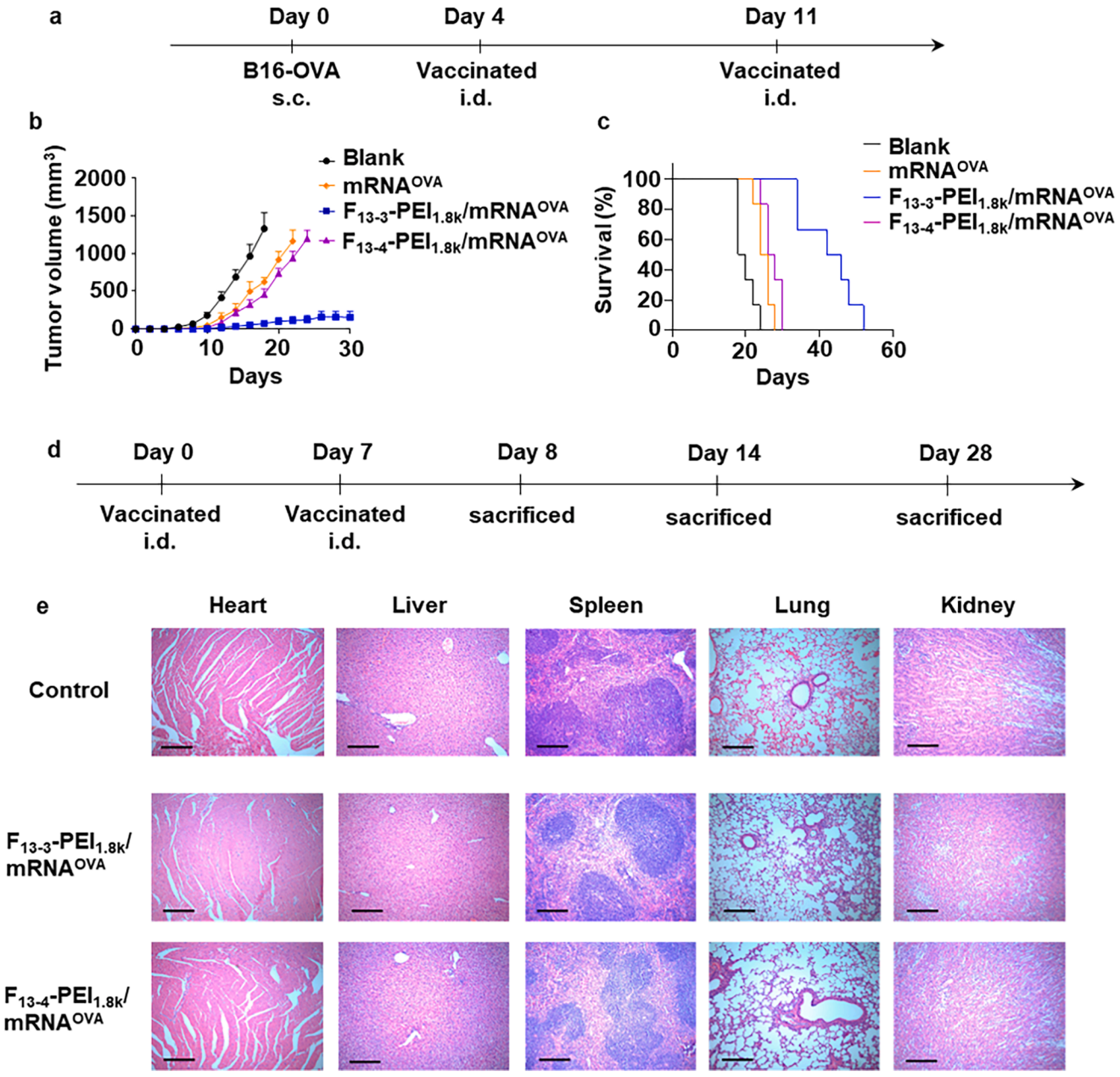

Fig. 5. F-PEI/$mRNA^{OVA}$ nanovaccine inhibits tumor growth and prolongs survival in tumor-bearing mice. (a) A scheme of tumor challenge experiment design (n = 6). (b) Tumor growth curves for B16-OVA on mice after the various treatments. The data show mean ± s.e.m. (c) Survival curves of mice bearing B16-OVA tumor in different treatment groups. (d) Timeline of the vaccination and H&E staining experiment of mice major organs. (e) H&E staining of major organs collected from vaccinated mice on Day 8. Major organs from untreated healthy mice of the same age were collected on Day 28 as control. Scale bar = 200 μm. s.c., subcutaneous; i.d., intradermal.

the splenocytes was analyzed on Day 14 (Fig. 4a). Notably, compared with the mRNA^{OVA} group and the F_{13}-PEI$_{1.8k}$-2/mRNA^{OVA} group, the frequency of SIINFEKL-MHC-I tetramer^{+}CD8^{+} T cells in the F_{13}-PEI$_{1.8k}$-1/mRNA^{OVA} group increased by 6.7-fold and 3.2-fold, respectively (Fig. 4d & 4e), suggesting that F_{13}-PEI$_{1.8k}$-1/mRNA^{OVA} vaccination could trigger the most robust OVA-specific immune responses.

Splenocytes from the twice-immunized mice were then restimulated with OVA antigen peptide (SIINFEKL), and OVA-specific T cell responses were examined. Compared with the mRNA^{OVA} group and the F_{13}-PEI$_{1.8k}$-2/mRNA^{OVA} group, the F_{13}-PEI$_{1.8k}$-1/mRNA^{OVA} group triggered the strongest IFN-γ responses, as evidenced by the highest level of IFN-γ producing cells from the enzyme-linked immunospot assay (ELISPOT) (Fig. 4f & 4 g) and the flow cytometry analysis (Fig. 4h). The results again indicated that the F_{13}-PEI$_{1.8k}$-1/mRNA^{OVA} vaccine triggered a strong OVA-specific T cell immune response *in vivo*.

Based on the strong antigen-specific immune responses induced by F-PEI/mRNA, we further assessed its antitumor efficacy. C57BL/6 mice were subcutaneously inoculated with B16-OVA cells to establish the

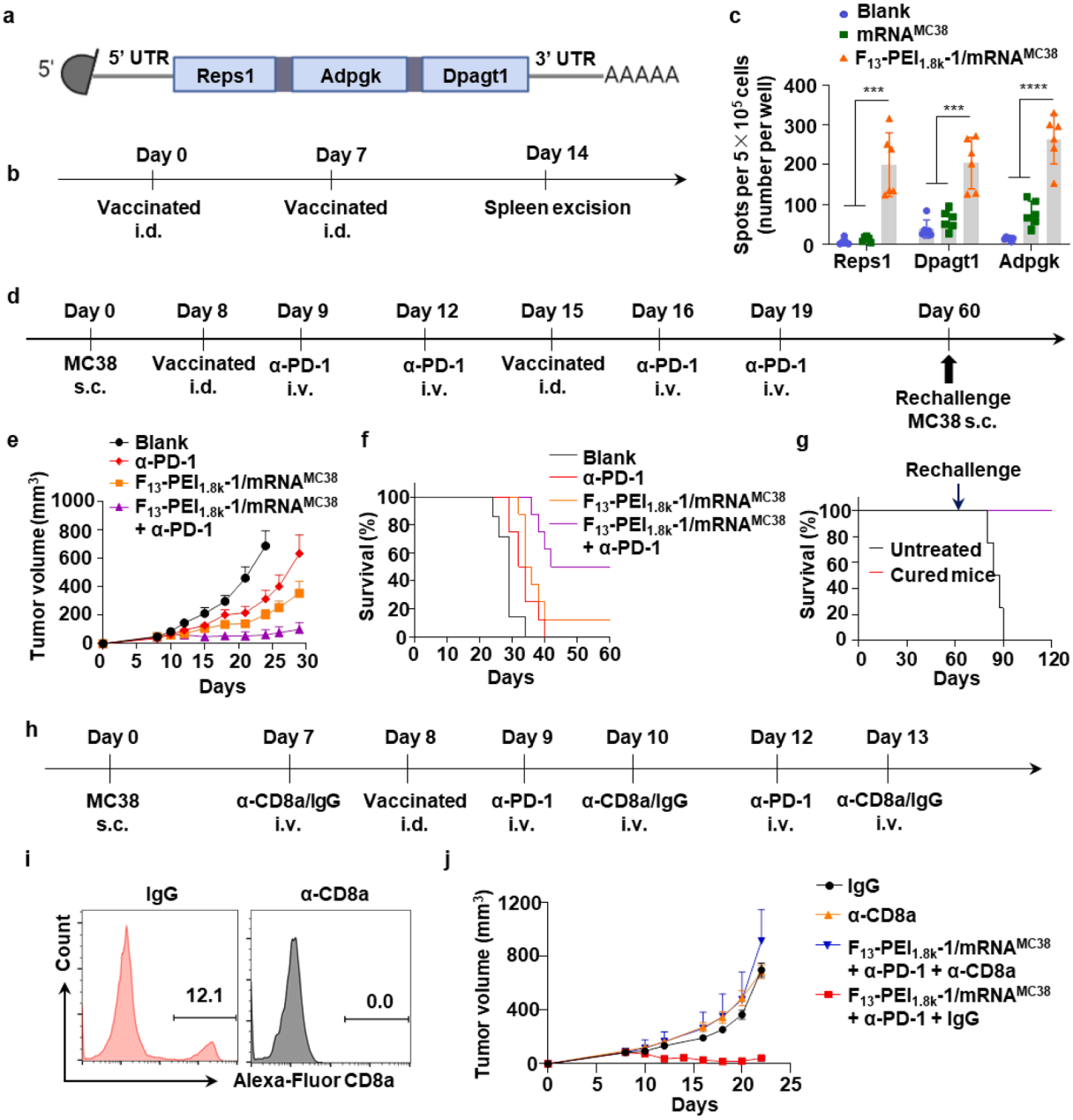

Fig. 6. F-PEI-based neoantigen mRNA vaccine for personalized immunotherapy. (a) Design of the MC38 tumor neoantigen mRNA vaccine. (b) C57BL/6 mice were immunized with the indicated formulations (PBS, mRNA^{MC38}, and F_{13}-PEI$_{1.8k}$-1/mRNA^{MC38}, 10 μg mRNA^{MC38} per mouse). (c) Statistical data of IFN-γ producing cells among splenocytes after *ex vivo* restimulation with peptide antigens on Day 14 post immunization (6 mice for each group, data shown as mean ± s.d.). (d) The timeline of F_{13}-PEI$_{1.8k}$-1/mRNA^{MC38} nanovaccine treatment combined with anti-PD-1 therapy. (e&f) Tumor growth curves (e) and survival curves (f) of mice in different treatment groups (data shown as mean ± s.e.m.) (g) Survival curves of the 4 cured mice (from 6f, the F_{13}-PEI$_{1.8k}$-1/mRNA^{MC38} vaccine + anti-PD-1 combination treatment group) rechallenged with MC38 cells on Day 60. Untreated: healthy mice of the same age challenged with MC38 cells. (h) The timeline of CD8^{+} T cell depletion experiment. (i) Flow cytometry analysis of CD8^{+} T cells in the mouse blood on the third day after treatment with anti-CD8a or an isotype mouse monoclonal antibody (IgG). (j) Tumor growth curves of the tumor-bearing mice pre-treated with either anti-CD8a or IgG followed by the combined F_{13}-PEI$_{1.8k}$-1/mRNA^{MC38} + anti-PD-1 therapy (data shown as mean ± s.d.). e,f,j, 7–8 mice for each group. Statistical significance between the indicated groups was determined using two-sided unpaired t-tests. ***P < 0.001, ****P < 0.0001. s.c., subcutaneous; i.d., intradermal; i.v., intravenous.

tumor-bearing mouse model. The mice were then treated two times with either phosphate buffered saline (PBS), $mRNA^{OVA}$, F_{13}-$PEI_{1.8k}$-1/$mRNA^{OVA}$ or F_{13}-$PEI_{1.8k}$-2/$mRNA^{OVA}$ at 1 week interval after 4 days (Fig. 5a). It could be observed that the F_{13}-$PEI_{1.8k}$-1/$mRNA^{OVA}$ cancer vaccine showed a strong tumor suppressive effect and effectively prolonged the survival time of mice (Fig. 5b & 5c), suggesting that the F_{13}-$PEI_{1.8k}$-1/$mRNA^{Ag}$ had the potential to be a therapeutic mRNA cancer vaccine.

Hematoxylin and eosin (H&E) staining of major organs of the F_{13}-$PEI_{1.8k}$-1/$mRNA^{OVA}$ or F_{13}-$PEI_{1.8k}$-2/$mRNA^{OVA}$ vaccinated mice showed no obvious sign of any acute organ damage or inflammatory lesions in mice on Day 8, Day 14, and Day 28 (Fig. 5d, 5e and Supplementary Fig. S2), suggesting the good biosafety of our treatment in mice.

3.4. F-PEI-based neoantigen mRNA vaccination combined with immune checkpoint blockade for personalized cancer therapy

Tumor neoantigens are non-self antigens produced by somatic cell mutations[32]. They only exist in cancer cells, not in normal cells[33]. Tumor neoantigens are highly immunogenic and can drive effective antitumor immune responses [34,35], and thus are showing strong prospects in the design of cancer vaccines [36–38]. In order to prove the applicability of our cancer vaccine platform, we constructed F-PEI-based neoantigen vaccines to treat MC38 colon cancer model. It has been reported that the MC38 tumor cell line-specific mutant peptides Reps1, Dpagt1 and Adpgk could be used as neoepitopes for T cells [39], and these mutant peptides could trigger specific $CD8^+$ T cell responses [40,41]. The encoding sequences of Reps1, Dpagt1 and Adpgk peptides were included in the open reading frame (ORF) of the mRNA to construct the MC38 neoantigen mRNA ($mRNA^{MC38}$) (Fig. 6a).

Next, we selected F_{13}-$PEI_{1.8k}$-1, which performed better in the previous experiments, as the neoantigen mRNA delivery vehicle. We simply mixed $mRNA^{MC38}$ with F_{13}-$PEI_{1.8k}$-1 to synthesize the F_{13}-$PEI_{1.8k}$-1/$mRNA^{MC38}$ nanovaccine with an average size of ~250 nm and a zeta potential of −6.8 mV (Supplementary Fig. S3). Compared with the control group and the $mRNA^{MC38}$ group, the splenocytes from mice immunized with F_{13}-$PEI_{1.8k}$-1/$mRNA^{MC38}$ showed significantly increased IFN-γ producing cells after restimulation with Reps1, Dpagt1 and Adpgk peptides, respectively, indicating that F_{13}-$PEI_{1.8k}$-1/$mRNA^{MC38}$ could induce potent antigen specific $CD8^+$ T cell responses for each displayed antigen (Fig. 6b & 6c).

The F_{13}-$PEI_{1.8k}$-1/$mRNA^{MC38}$ cancer vaccine was then combined with the immune checkpoint inhibitor anti-PD-1 to evaluate its antitumor effect (Fig. 6d). It could be seen that the tumor growth in F_{13}-$PEI_{1.8k}$-1/$mRNA^{MC38}$ immunized mice was significantly delayed compared with the mice in the control group and the anti-PD-1 group. Moreover, the combined treatment with anti-PD-1 could further improve the antitumor therapeutic effect of F_{13}-$PEI_{1.8k}$-1/$mRNA^{MC38}$ vaccine (Fig. 6e). In fact, F_{13}-$PEI_{1.8k}$-1/$mRNA^{MC38}$ combined with anti-PD-1 treatment significantly prolonged the survival time of mice (Fig. 6f), and 50 % of mice showed complete tumor regression. Notably, when mice that survived from the combinational treatment were rechallenged with MC38 cells on Day 60, compared to healthy mice challenged with MC38 cells (the untreated group), 100 % of the cured mice survived (Fig. 6g), indicating effective immunological memory effect triggered by the F_{13}-$PEI_{1.8k}$-1/$mRNA^{MC38}$ combined with anti-PD-1 treatment against tumor recurrence.

In order to verify the importance of $CD8^+$ T cells in the combination therapy, anti-CD8a was used to perform the $CD8^+$ T cell depletion experiment (Fig. 6h). The depletion of $CD8^+$ T cells in the peripheral blood of mice was analyzed by flow cytometry on the third day after intravenous injection of anti-CD8a or mouse IgG (as control). The results showed complete depletion of $CD8^+$ T cells from the peripheral blood of mice treated with anti-CD8a, while $CD8^+$ T cells in the mice treated with mouse IgG remain unaffected (Fig. 6i). As expected, after $CD8^+$ T cell depletion, the inhibitory effect of the combination therapy on tumor growth was dramatically impaired (Fig. 6j), suggesting that $CD8^+$ T cells played a key role in the tumor suppression by the combination therapy.

4. Conclusions

In this work, we synthesized fluoroalkane modified cationic polymers for mRNA vaccine delivery and immune stimulation. We established a fluorinated polymer-based mRNA nanovaccine platform, by simple blending of F-PEI with mRNA encoding antigen(s). Our fluorinated polymer-based mRNA vaccine could effectively promote the uptake of mRNA by DCs, activate the TLR4 signaling pathway, trigger the DC activation and antigen presentation by DCs, therefore induce T cell priming, stimulate the tumor antigen-specific cellular immunity, and significantly delay the tumor growth after therapeutic vaccination. We further combined the fluorinated polymer-based MC38 neoantigen mRNA vaccine with the immune checkpoint inhibitor, and eradicated tumors in 50 % of the MC38 tumor-bearing mice and successfully prevented tumor reoccurrence. In conclusion, we have developed a novel cancer vaccine platform suitable for the delivery of mRNA vaccines, and demonstrated synergistic therapeutic effects of such personalized neoantigen vaccines in combination with immune checkpoint inhibitors. In the future, the mRNA delivery polymer developed in this work might be extended to applications in other mRNA-based therapeutics where high level of mRNA delivery is desired, or both robust cellular and humoral immune responses are crucial, e.g., in the fight against viral infections, besides neutralizing antibody induction, strong cellular immune responses are required to eliminate the infected cells.

Declaration of Competing Interest

The authors declare that they have no known competing financial interests or personal relationships that could have appeared to influence the work reported in this paper.

Data availability

No data was used for the research described in the article.

Acknowledgements

This work is dedicated to the memory of Dr. Jun Xu, who passed away in a tragic accident. Jun took part in the original design, the functionalization & optimization of the F-PEI polymers, and several efficacy evaluation assays. This work was partially supported by the National Key Research and Development (R&D) Program of China (2022YFB3804604 and 2021YFF0701800), the National Natural Science Foundation of China (32071382, 52032008, and 21927803), the Natural Science Foundation of Jiangsu Higher Education Institutions of China (19KJA310008), Suzhou Science and Technology Development Project-Science and Technology Innovation in Medicine and Health Care (SKY2021033), the Collaborative Innovation Center of Suzhou Nano Science and Technology (Nano-CIC), the 111 Project, the National Center of Technology Innovation for Biopharmaceuticals (NCTIB2022HS01011), and the Suzhou Key Laboratory of Nanotechnology and Biomedicine.

Appendix A. Supplementary data

Supplementary data to this article can be found online at https://doi.org/10.1016/j.cej.2022.140930.

References

[1] K. Vermaelen, Vaccine strategies to improve anti-cancer cellular immune responses, Front. Immunol. 10 (2019) 00008.

[2] C.G. Kim, Y.B. Sang, J.H. Lee, H.J. Chon, combining cancer vaccines with immunotherapy: establishing a new immunological approach, Int. J. Mol. Sci. 22 (2021) 8035.
[3] Q.L. Zhang, S. Hong, X. Dong, D.W. Zheng, J.L. Liang, X.F. Bai, X.N. Wang, Z. Y. Han, X.Z. Zhang, Bioinspired nano-vaccine construction by antigen pre-degradation for boosting cancer personalized immunotherapy, Biomaterials 287 (2022), 121628.
[4] Z. Deng, Y. Tian, J. Song, G. An, P. Yang, mRNA vaccines: the dawn of a new era of cancer immunotherapy, Front. Immunol. 13 (2022), 887125.
[5] J. Shi, M.W. Huang, Z.D. Lu, X.J. Du, S. Shen, C.F. Xu, J. Wang, Delivery of mRNA for regulating functions of immune cells, J. Control. Release 345 (2022) 494–511.
[6] M. Moser, O. Leo, Key concepts in immunology, Vaccine 28 (2010) C2–C13.
[7] V. Appay, D.C. Douek, D.A. Price, CD8(+) T cell efficacy in vaccination and disease, Nat. Med. 14 (2008) 623–628.
[8] X. Ji, D. Guo, J. Ma, M. Yin, Y. Yu, C. Liu, Y. Zhou, J. Sun, Q. Li, N. Chen, C. Fan, H. Song, Epigenetic remodeling hydrogel patches for multidrug-resistant triple-negative breast cancer, Adv. Mater. 33 (18) (2021) 2100949.
[9] P.J. Eggenhuizen, B.H. Ng, J.D. Ooi, Antigen-driven CD4(+) T-cell anergy: a pathway to peripheral T regulatory cells, Immunol. Cell Biol. 99 (2021) 252–254.
[10] S. Linares-Fernandez, C. Lacroix, J.Y. Exposito, B. Verrier, Tailoring mRNA vaccine to balance innate/adaptive immune response, Trends Mol. Med. 26 (2020) 311–323.
[11] N. Pardi, M.J. Hogan, F.W. Porter, D. Weissman, mRNA vaccines - a new era in vaccinology, Nat. Rev. Drug Discov. 17 (2018) 261–279.
[12] Q. Shuai, F.T. Zhu, M.D. Zhao, Y.F. Yan, mRNA delivery via non-viral carriers for biomedical applications, Int J Pharmaceut 607 (2021), 121020.
[13] N. Pardi, M.J. Hogan, D. Weissman, Recent advances in mRNA vaccine technology, Curr. Opin. Immunol. 65 (2020) 14–20.
[14] Y. Yin, X. Li, H. Ma, J. Zhang, D. Yu, R. Zhao, S. Yu, G. Nie, H. Wang, In situ transforming RNA nanovaccines from polyethylenimine functionalized graphene oxide hydrogel for durable cancer immunotherapy, Nano Lett. 21 (2021) 2224–2231.
[15] F.P. Polack, S.J. Thomas, N. Kitchin, J. Absalon, A. Gurtman, S. Lockhart, J. L. Perez, G.P. Marc, E.D. Moreira, C. Zerbini, R. Bailey, K.A. Swanson, S. Roychoudhury, K. Koury, P. Li, W.V. Kalina, D. Cooper, R.W. Frenck, L. L. Hammitt, O. Tureci, H. Nell, A. Schaefer, S. Unal, D.B. Tresnan, S. Mather, P. R. Dormitzer, U. Sahin, K.U. Jansen, W.C. Gruber, C.C.T. Grp, Safety and efficacy of the BNT162b2 mRNA covid-19 vaccine, New Engl J Med 383 (2020) 2603–2615.
[16] L.R. Baden, H.M. El Sahly, B. Essink, K. Kotloff, S. Frey, R. Novak, D. Diemert, S. A. Spector, N. Rouphael, C.B. Creech, J. McGettigan, S. Khetan, N. Segall, J. Solis, A. Brosz, C. Fierro, H. Schwartz, K. Neuzil, L. Corey, P. Gilbert, H. Janes, D. Follmann, M. Marovich, J. Mascola, L. Polakowski, J. Ledgerwood, B.S. Graham, H. Bennett, R. Pajon, C. Knightly, B. Leav, W.P. Deng, H.H. Zhou, S. Han, M. Ivarsson, J. Miller, T. Zaks, C.S. Grp, Efficacy and safety of the mRNA-1273 SARS-CoV-2 vaccine, New Engl J Med 384 (2021) 403–416.
[17] X.C. Hou, T. Zaks, R. Langer, Y.Z. Dong, Lipid nanoparticles for mRNA delivery, Nat. Rev. Mater. 7 (2022) 65.
[18] M.J.W. Evers, J.A. Kulkarni, R. van der Meel, P.R. Cullis, P. Vader, R.M. Schiffelers, State-of-the-art design and rapid-mixing production techniques of lipid nanoparticles for nucleic acid delivery, Small Methods 2 (9) (2018).
[19] S.-D. Xiong, L. Li, J. Jiang, L.-P. Tong, S. Wu, Z.-S. Xu, P.K. Chu, Cationic fluorine-containing amphiphilic graft copolymers as DNA carriers, Biomaterials 31 (9) (2010) 2673–2685.
[20] M.M. Wang, Y.Y. Cheng, Structure-activity relationships of fluorinated dendrimers in DNA and siRNA delivery, Acta Biomater. 46 (2016) 204–210.
[21] J.H. Zhang, W.J. Wang, J. Zhang, Y.P. Xiao, Y.H. Liu, X.Q. Yu, ROS-responsive fluorinated polycations as non-viral gene vectors, Eur. J. Med. Chem. 182 (2019), 111666.
[22] Z.J. Zhang, W.W. Shen, J. Ling, Y. Yan, J.J. Hu, Y.Y. Cheng, The fluorination effect of fluoroamphiphiles in cytosolic protein delivery, Nat. Commun. 9 (2018) 1377.
[23] I.T. Horvath, J. Rabai, Facile catalyst separation without water - fluorous biphase hydroformylation of olefins, Science 266 (1994) 72–75.
[24] M. Cametti, B. Crousse, P. Metrangolo, R. Milani, G. Resnati, The fluorous effect in biomolecular applications, Chem. Soc. Rev. 41 (2012) 31–42.
[25] M.C.Z. Kasuya, S. Nakano, R. Katayama, K. Hatanaka, Evaluation of the hydrophobicity of perfluoroalkyl chains in amphiphilic compounds that are incorporated into cell membrane, J. Fluor. Chem. 132 (2011) 202–206.
[26] M.M. Wang, H.M. Liu, L. Li, Y.Y. Cheng, A fluorinated dendrimer achieves excellent gene transfection efficacy at extremely low nitrogen to phosphorus ratios, Nat. Commun. 5 (2014) 3053.
[27] J. Xu, J. Lv, Q. Zhuang, Z.J. Yang, Z.Q. Cao, L.G. Xu, P. Pei, C.Y. Wang, H.F. Wu, Z. L. Dong, Y. Chao, C. Wang, K. Yang, R. Peng, Y.Y. Cheng, Z. Liu, A general strategy towards personalized nanovaccines based on fluoropolymers for post-surgical cancer immunotherapy, Nat. Nanotechnol. 15 (2020) 1043–1052.
[28] A. Hall, U. Lachelt, J. Bartek, E. Wagner, S.M. Moghimi, Polyplex evolution: understanding biology, optimizing performance, Mol. Ther. 25 (2017) 1476–1490.
[29] A.P. Pandey, K.K. Sawant, Polyethylenimine: a versatile, multifunctional non-viral vector for nucleic acid delivery, Mater. Sci. Eng. C, Mater. Biol. Appl. 68 (2016) 904–918.
[30] F. Steinhagen, T. Kinjo, C. Bode, D.M. Klinman, TLR-based immune adjuvants, Vaccine 29 (2011) 3341–3355.
[31] M.A. Shetab Boushehri, A. Lamprecht, TLR4-based immunotherapeutics in cancer: a review of the achievements and shortcomings, Mol. Pharm. 15 (2018) 4777–4800.
[32] P. Xu, H. Luo, Y. Kong, W.-F. Lai, L. Cui, X. Zhu, Cancer neoantigen: boosting immunotherapy, Biomed. Pharmacother. 131 (2020) 110640.
[33] U. Sahin, O. Tureci, Personalized vaccines for cancer immunotherapy, Science 359 (2018) 1355–1360.
[34] D. Perumal, N. Imai, A. Lagana, J. Finnigan, D. Melnekoff, V.V. Leshchenko, A. Solovyov, D. Madduri, A. Chari, H.J. Cho, J.T. Dudley, J.D. Brody, S. Jagannath, B. Greenbaum, S. Gnjatic, N. Bhardwaj, S. Parekh, Mutation-derived Neoantigen-specific T-cell Responses in Multiple Myeloma, Clin. Cancer Res. 26 (2020) 450–464.
[35] M. Yarchoan, B.A. Johnson, E.R. Lutz, D.A. Laheru, E.M. Jaffee, Targeting neoantigens to augment antitumour immunity (vol 17, pg 209, 2017), Nat. Rev. Cancer 17 (2017) 569.
[36] E. Blass, P.A. Ott, Advances in the development of personalized neoantigen-based therapeutic cancer vaccines, Nat. Rev. Clin. Oncol. 18 (2021) 215–229.
[37] P.A. Ott, Z.T. Hu, D.B. Keskin, S.A. Shukla, J. Sun, D.J. Bozym, W.D. Zhang, A. Luoma, A. Giobbie-Hurder, L. Peter, C. Chen, O. Olive, T.A. Carter, S.Q. Li, D. J. Lieb, T. Eisenhaure, E. Gjini, J. Stevens, W.J. Lane, I. Javeri, K. Nellaiappan, A. M. Salazar, H. Daley, M. Seaman, E.I. Buchbinder, C.H. Yoon, M. Harden, N. Lennon, S. Gabriel, S.J. Rodig, D.H. Barouch, J.C. Aster, G. Getz, K. Wucherpfennig, D. Neuberg, J. Ritz, E.S. Lander, E.F. Fritsch, N. Hacohen, C. J. Wu, An immunogenic personal neoantigen vaccine for patients with melanoma, Nature 547 (2017) 217–221.
[38] G. Cafri, J.J. Gartner, T. Zaks, K. Hopson, N. Levin, B.C. Paria, M.R. Parkhurst, R. Yossef, F.J. Lowery, M.S. Jafferji, T.D. Prickett, S.L. Goff, C.T. McGowan, S. Seitter, M.L. Shindorf, A. Parikh, P.D. Chatani, P.F. Robbins, S.A. Rosenberg, mRNA vaccine-induced neoantigen-specific T cell immunity in patients with gastrointestinal cancer, J. Clin. Invest. 130 (2020) 5976–5988.
[39] M. Yadav, S. Jhunjhunwala, Q.T. Phung, P. Lupardus, J. Tanguay, S. Bumbaca, C. Franci, T.K. Cheung, J. Fritsche, T. Weinschenk, Z. Modrusan, I. Mellman, J. R. Lill, L. Delamarre, Predicting immunogenic tumour mutations by combining mass spectrometry and exome sequencing, Nature 515 (2014) 572–576.
[40] R. Kuai, L.J. Ochyl, K.S. Bahjat, A. Schwendeman, J.J. Moon, Designer vaccine nanodiscs for personalized cancer immunotherapy, Nat. Mater. 16 (2017) 489–496.
[41] W.J. Wang, Z.D. Liu, X.X. Zhou, Z.Q. Guo, J. Zhang, P. Zhu, S. Yao, M.Z. Zhu, Ferritin nanoparticle-based SpyTag/SpyCatcher-enabled click vaccine for tumor immunotherapy, Nanomed-Nanotechnol. 16 (2019) 69–78.